JACS
JOURNAL OF THE AMERICAN CHEMICAL SOCIETY
pubs.acs.org/JACS
Article

Active, Yet Little Mobility: Asymmetric Decomposition of H_2O_2 Is Not Sufficient in Propelling Catalytic Micromotors

Xianglong Lyu, Xiaoxia Liu, Chao Zhou, Shifang Duan, Pengzhao Xu, Jia Dai, Xiaowen Chen, Yixin Peng, Donghao Cui, Jinyao Tang, Xing Ma,* and Wei Wang*

Cite This: J. Am. Chem. Soc. 2021, 143, 12154–12164

Read Online

ACCESS | Metrics & More | Article Recommendations | Supporting Information

ABSTRACT: A popular principle in designing chemical micromachines is to take advantage of asymmetric chemical reactions such as the catalytic decomposition of H_2O_2. Contrary to intuition, we use Janus micromotors half-coated with platinum (Pt) or catalase as an example to show that this ingredient is not sufficient in powering a micromotor into self-propulsion. In particular, by annealing a thin Pt film on a SiO_2 microsphere, the resulting microsphere half-decorated with discrete Pt nanoparticles swims ~80% more slowly than its unannealed counterpart in H_2O_2, even though they both catalytically produce comparable amounts of oxygen. Similarly, SiO_2 microspheres half-functionalized with the enzyme catalase show negligible self-propulsion despite high catalytic activity toward decomposing H_2O_2. In addition to highlighting how surface morphology of a catalytic cap enables/disables a chemical micromotor, this study offers a refreshed perspective in understanding how chemistry powers nano- and microscopic objects (or not): our results are consistent with a self-electrophoresis mechanism that emphasizes the electrochemical decomposition of H_2O_2 over nonelectrochemical pathways. More broadly, our finding is a critical piece of the puzzle in understanding and designing nano- and micromachines, in developing capable model systems of active colloids, and in relating enzymes to active matter.

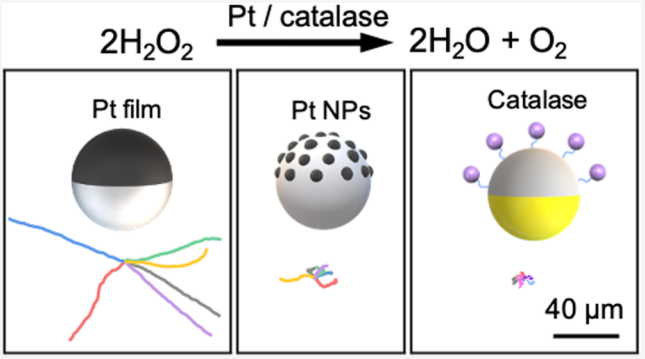

INTRODUCTION

Over the last 2 decades, micromotors that harvest environmental energy and move autonomously, also known as "synthetic microswimmers" or "active colloids", have received mounting interest.[1−4] For applications, micromotors demonstrate promising potentials in drug delivery, biosensing, environmental monitoring and remediation, and microfabrication.[5−8] On a fundamental level, soft matter physicists use micromotors (or "active colloids") as a model system to study active matter.[9−11] From either a fundamental or applied point of view, it is essential to understand how a micromotor moves, which is sometimes deceptively elusive.

One archetypical micromotor that has enjoyed particular popularity and success across different fields or research is made of an inert microsphere half-coated with platinum (Pt), which catalyzes the decomposition of H_2O_2 via[12,13]

$$2H_2O_2 \xrightarrow{Pt} 2H_2O + O_2$$

The discovery of this Pt-coated micromotor in 2007[12] inspired numerous designs that are asymmetrically covered/loaded with catalytically active species, such as MnO_2,[14] Ag,[15−17] Pt nanoparticles,[18−20] enzymes,[21−25] or other precious metals such as Pd and Ir,[26,27] which all catalyzes the decomposition of H_2O_2 into O_2. This list of successful micromotors leaves the impression that a micromotor can self-propel as long as H_2O_2 is asymmetrically decomposed on the particle surface. Because this idea is simple and intuitive, it has arguably gained a foothold among many of us who are new to this research field or those who pay more attention to the usefulness rather than the exact mechanisms of micromotors.

In this article, we show compelling evidence that fast asymmetric catalysis does NOT guarantee strong self-propulsion. Specifically, we present counterintuitive results that microspheres half-coated with discrete Pt nanoparticles (instead of a continuous Pt film), or coated with the enzyme catalase, do not self-propel significantly beyond Brownian motion, even though both *actively and asymmetrically* catalyze the decomposition of H_2O_2 into water and O_2. By careful measurements and numerical simulations, this observation can be reconciled with a "self-electrophoresis" mechanism that highlights the electrochemical pathway of H_2O_2 decomposi-

Received: May 3, 2021
Published: August 2, 2021

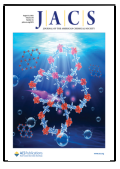

Downloaded via UNIV TOWN OF SHENZHEN on August 31, 2021 at 05:40:08 (UTC).
See https://pubs.acs.org/sharingguidelines for options on how to legitimately share published articles.

© 2021 American Chemical Society

https://doi.org/10.1021/jacs.1c04501
J. Am. Chem. Soc. 2021, 143, 12154−12164

tion. This study provides paradigm-shifting insights in understanding chemical propulsion at microscopic scales and in the design of chemical micro- and nanomotors.

EXPERIMENTAL SECTION

Materials and Instruments. Hydrogen peroxide (H_2O_2, 30 wt %) was purchased from Alfa Aesar. Ethanol (CH_3CH_2OH) and isopropyl alcohol (C_3H_8O) were purchased from Aladin, China. Silica (SiO_2) microspheres were purchased from Tianjin Baseline Chromtech Research Center, China. 3-Aminopropyltriethoxysiane (APTES), glutaraldehyde (GA), fluorescein isothiocyanate (FITC), and catalase from bovine liver (C1345-1G, 2 000−5 000 units/mg protein) were purchased from Sigma-Aldrich, Germany. A high vacuum sputter machine (Leica EM ACE600) was used to coat platinum or gold on silica microspheres and silicon wafers. A field-emission scanning electron microscope (FESEM; Zeiss SUPRA 55) and a confocal laser scanning microscope (Nikon A1) were used for imaging. A high-temperature tube furnace (Kejing, OTF-1200X-S) was used to anneal samples. A spectrometer (UV-3600 Shimadzu) was used to measure the adsorption spectra of SiO_2-catalase in the bicinchoninic acid (BCA) protein assay kit. The zeta potential of SiO_2−Pt was characterized by the Zetasizer NanoZS90.

Fabrication of SiO_2−Pt_{film} and SiO_2−Pt_{np} Janus Microspheres. A monolayer of SiO_2 spheres (5 μm in diameter) was first prepared by a drop-casting method. SiO_2 spheres suspension was mixed with equal volumes of isopropyl alcohol, then the mixture was dispersed by ultrasound and drop-casted on a piece of wafer that has been precleaned by O_2 plasma (PCE-6 model) for 300 s. SiO_2−Pt_{film} Janus spheres with a zeta potential of ∼−22 mV were prepared by sputtering Pt of 10 nm on a monolayer of SiO_2 spheres in a chamber prefilled with argon, operating at a vacuum level of 6.77×10^{-3} Torr. To fabricate SiO_2−Pt_{np} Janus spheres, these SiO_2−Pt_{film} Janus spheres were annealed at 300, 600, or 900 °C at a heating rate of about 10 °C/min for 2 h in an argon atmosphere (99.999%). Note that the zeta potential of SiO_2−Pt microspheres remained largely unchanged after annealing (Figure S1).

Fabrication of SiO_2-Catalase Janus Microspheres. SiO_2−NH_2 microspheres were first synthesized by mixing 1 mL of SiO_2 (2.5 wt %, 5 μm in diameter), 1 mL of ethanol, and 10 μL of APTES and were shaken to mix for 24 h. The prepared SiO_2−NH_2 microspheres were then washed with ethanol three times. Then, a suspension of SiO_2−NH_2 microspheres was mixed with equal volumes of deionized (DI) water (18.2 MΩ cm) and drop-casted on a piece of glass that was precleaned by O_2 plasma for 300 s to form a monolayer of SiO_2−NH_2 microspheres. SiO_2−NH_2−Au Janus microspheres were prepared by sputtering ∼5 nm Au on the monolayer of SiO_2−NH_2 spheres. The SiO_2−NH_2−Au Janus microspheres were ultrasonically dispersed into a mixed solution containing 1 mL of PBS buffer solution (pH = 6.8) and 50 μL of glutaraldehyde (GA) and reacted for 3 h. GA served as the link between the amine functional groups on a microsphere and catalase. After washing with PBS buffer solution, the SiO_2−NH_2−Au Janus microspheres were redispersed to a PBS buffer solution containing 5 mg/mL of catalase, which were allowed to react overnight to obtain catalase-functionalized Janus SiO_2 microspheres (catalase was only functionalized on the half of the microsphere that was not covered with gold). Finally, the SiO_2-catalase Janus spheres were washed with DI H_2O and stored at 4 °C before use. The preparation process of the catalase-functionalized glass slide was the same as SiO_2-catalase microspheres, except that the glass slide was treated with O_2 plasma for 600 s before being modified with catalase.

In case fluorescent catalase was needed, 0.5 mg of FITC and 20 mg of catalase was dissolved in PBS buffer solution (0.1 M, pH = 9.2), and the solution was allowed to react for 4 h in darkness at room temperature. Then, the fluorescein-tagged catalase was obtained after removing unreacted FITC by placing the product in a dialysis bag (3.5 kDa pore membrane) for 24 h.

Determination of the Amount of Catalase Modified on a SiO_2 Sphere. A BCA protein assay kit was used to determine the amount of catalase functionalized on a SiO_2 sphere.[28] At a basic pH, the peptide bond of a protein molecule complexes with Cu^{2+} and reduces it to Cu^+ that specifically bonds with BCA to form a stable purple-blue complex. Because its light absorption value at 562 nm is proportional to the protein concentration, a calibration curve (Figure S2) is made, from which the measured absorption of a protein solution of an unknown concentration can be obtained. In our experiment, 20 μL of SiO_2 or SiO_2-catalase suspension were mixed with 200 μL of BCA working solution, respectively. Then, the resulting mixtures were kept in a water bath of 37 °C for 30 min. The catalase content was finally quantified by UV−vis spectroscopy at 562 nm after they were cooled to room temperature.

Measurement of Oxygen Evolution Rate. A drainage method from ref 29 was adapted to measure the amount of O_2 generated from Pt-coated substrates in H_2O_2, and a scheme is shown in Figure S3. Three types of samples were tested: silicon wafer pieces (2 cm × 2 cm) sputtered with Pt of different thicknesses (5, 10, 20 nm), silicon wafers pieces (2 cm × 2 cm) sputtered with 10 nm of Pt but annealed at different temperatures (300, 600, and 900 °C), or a piece catalase-functionalized glass slide (2 cm × 1.5 cm). In a typical measurement, the sample was first placed at the bottom of a round-bottom flask, to which 4 mL of H_2O and 2 mL of 30 wt % H_2O_2 were then added sequentially. The suspension was then stirred at 500 rpm to promote the mixing of the solution and the release of oxygen. The generated O_2 was collected via a rubber tube by a graduated cylinder placed upside down in a water-filled tank. The O_2 evolution rate E_{O_2} was calculated by $E_{O_2} = V_{O_2}/V_m S\Delta t$, where V_{O_2} is the volume of O_2 at a constant time interval, Δt = 20 s, S is the sputtered area of silicon or glass, and V_m = 24.5 L/mol is the molar volume of gas at 25 °C, 101 kPa assuming an ideal gas.

Motion Experiment. The SiO_2−Pt_{film} and SiO_2−Pt_{np} Janus microspheres were scratched off the wafer and dispersed in DI water before use. Then, 10 μL of 30 wt % H_2O_2 solution was added into 20 μL of colloidal suspension to yield an aqueous solution of 5% H_2O_2 (the concentration can be varied by changing the volume of H_2O_2 added). The colloidal suspension was added to a piece of glass slide and observed from underneath with an inverted optical microscope (Olympus IX73). Videos with a typical length of 20 s were taken by a Point Grey camera (FL3-U3-13E4C-C) mounted on the microscope at a frame rate of 15 per second, then processed to obtain particles coordinates by MATLAB codes (courtesy of Prof. Hepeng Zhang from Shanghai Jiaotong University). Drift correction was performed by homemade MATLAB codes courtesy of Prof. Himanagamanasa Kandula from the University of Massachusetts.

Quantifying Motor Dynamics. The dynamics of micromotors were quantified by their mean squared displacement (MSD) following existing protocols.[12,30−32] To minimize errors, only the data of $\Delta t \leq 2$ s was used to plot the graph of MSD vs Δt, as shown in Figures S4−S6. The speeds of SiO_2−Pt_{film} and SiO_2−Pt_{np} motors were extracted by fitting the MSD vs Δt data with $\langle \Delta L^2 \rangle = 4D\Delta t + V^2\Delta t^2$. This equation is appropriate for the entire range of $\Delta t \leq 2$ s because the characteristic rotational time for 5 μm SiO_2 microspheres is ∼100 s. As a result, we are well in the ballistic regime for $\Delta t \leq 2$ s. For the catalase-functionalized Janus SiO_2 microspheres, their effective diffusivity D at different concentrations of H_2O_2 were obtained by fitting the MSD vs Δt data with $\langle \Delta L^2 \rangle = 4D\Delta t$ because of minimal self-propulsion.

RESULTS

Annealing a SiO_2−Pt Micromotor Significantly Reduces Its Speed. We begin with a quantitative comparison in speeds between silicon dioxide (SiO_2) microspheres half-coated with a continuous Pt film (referred to as "SiO_2−Pt_{film}" Janus micromotors hereafter) and those with discrete Pt nanoparticles ("SiO_2−Pt_{np}"). A scheme of their fabrication is illustrated in Figure 1a, and details are given in the Experimental Section. Very briefly, Pt films were physically deposited on a monolayer of SiO_2 microspheres. To fabricate SiO_2−Pt_{np}, SiO_2−Pt_{film} microspheres were thermally annealed

https://doi.org/10.1021/jacs.1c04501
J. Am. Chem. Soc. 2021, 143, 12154−12164

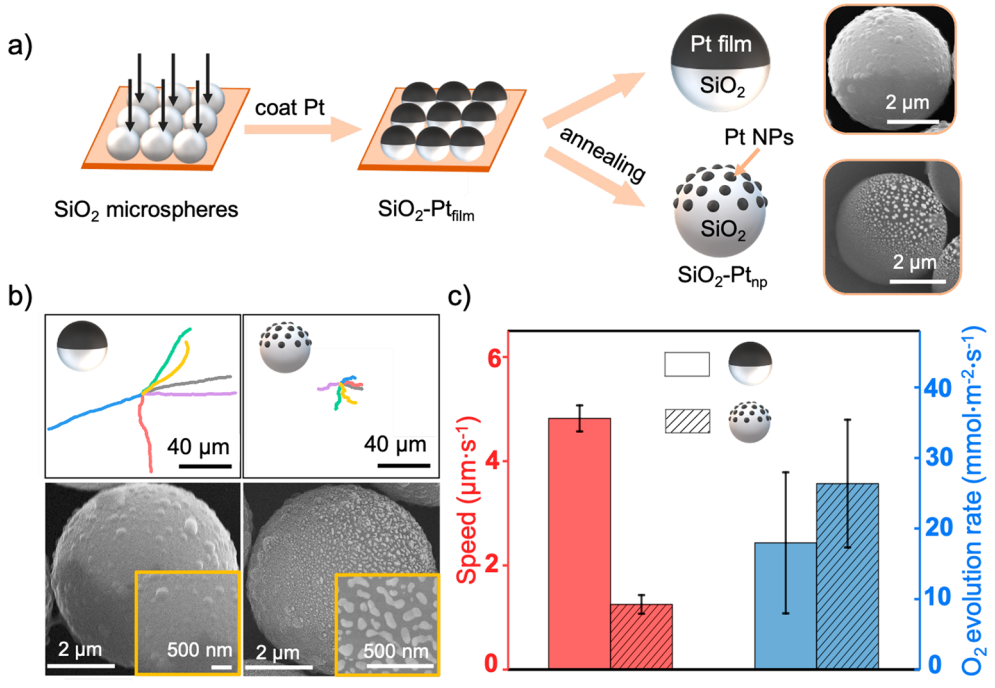

Figure 1. A Janus microsphere half-coated with platinum nanoparticles (Pt NPs) does not self-propel despite high catalytic activity. (a) Fabrication scheme via sputtering of a SiO_2−Pt Janus microsphere (SiO_2−Pt_{film}) and its conversion into one with discrete Pt nanoparticles (SiO_2−Pt_{np}) via annealing. (b) Top: representative trajectories for 20 s of a SiO_2−Pt_{film} (left) and a SiO_2−Pt_{np} micromotor (right) in 10 wt % H_2O_2. Bottom: scanning electron micrographs of the corresponding microspheres, highlighting the presence of nanoparticles on the Pt layer after annealing but not before. (c) Despite a significant difference in the propulsion speeds (left axis) between a SiO_2−Pt_{film} (not annealed) and a SiO_2−Pt_{np} micromotor (annealed at 600 °C), they are similarly active toward decomposing H_2O_2 into O_2 (see the Experimental Section for details).

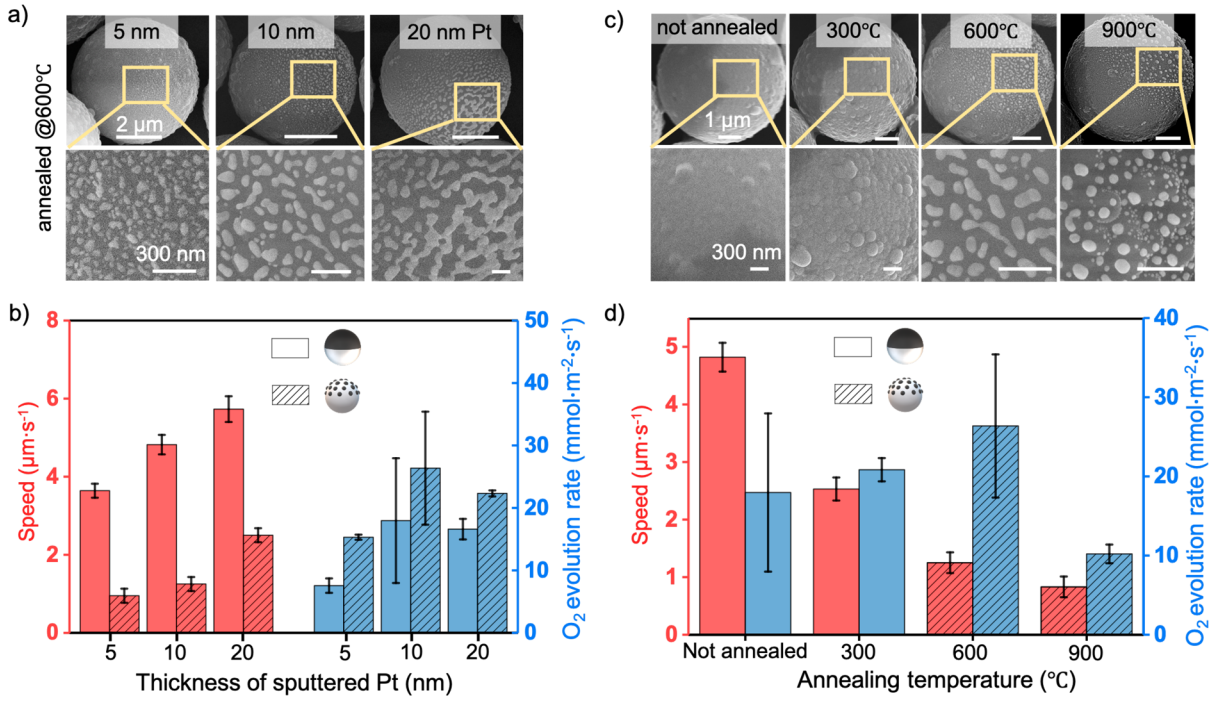

Figure 2. SiO_2−Pt micromotors fabricated by sputtering Pt films of different thickness (a and b, all annealed at 600 °C) or annealed at different temperatures (c and d, film thickness 10 nm). (a) Scanning electron micrographs of Pt films of different thicknesses after annealing, highlighting the surface morphologies in the zoomed-in views. (b) Speeds of SiO_2−Pt micromotors of different Pt thicknesses and their oxygen evolution rate. (c and d) Similar data for SiO_2−Pt microspheres before annealing and those annealed at 300, 600, and 900 °C.

in a furnace. The Pt film melted and then solidified into discrete Pt nanoparticles, which were still located on half of the SiO_2 microspheres (Figure S7).

Our key finding is that SiO_2−Pt_{np} moves surprisingly slowly in H_2O_2 (Figure 1b,c and Video S1). For example, trajectories of SiO_2−Pt_{np} acquired by annealing SiO_2−Pt_{film} at 600 °C for 2

https://doi.org/10.1021/jacs.1c04501
J. Am. Chem. Soc. 2021, 143, 12154−12164

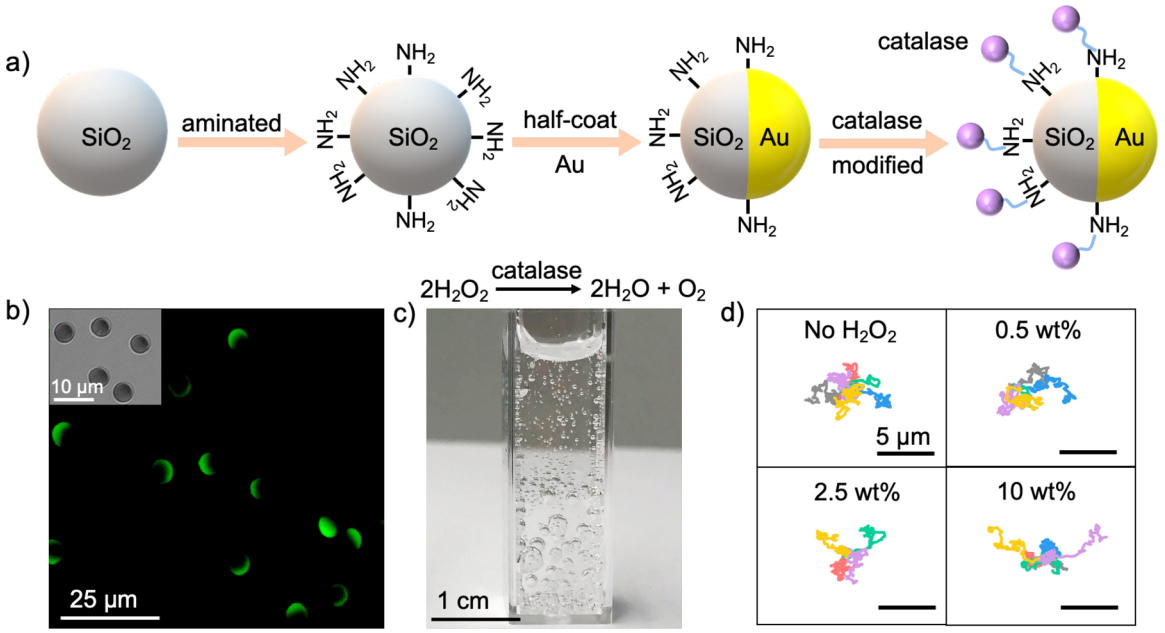

Figure 3. Experiments with catalase-coated Janus microspheres. (a) Fabrication scheme. A SiO_2 microsphere of 5 μm in diameter is first uniformly functionalized with amine functional groups, then half-coated with a thin layer of gold to block the amine groups on one hemisphere. The unblocked amine groups then bind with catalase, resulting in a SiO_2 microsphere half-functionalized with catalase ("SiO_2-catalse"). See the Experimental Section for fabrication details. (b) Confocal micrograph showing the parts on a SiO_2 microsphere functionalized with catalase (fluorescently labeled with FITC). Inset: the entire microspheres under bright field microscopy. (c) Bubble evolution from a cuvette filled with SiO_2-catalse microspheres (a population density of ~2.5 wt %) suspended in 1 wt % H_2O_2, after a period of ~1200 s. (d) Representative tracked trajectories (after drift correction) over a period of 20 s for a few SiO_2-catalse in H_2O_2 of different concentrations.

h are compared in Figure 1b with those unannealed in 10% H_2O_2, a typical concentration used in the literature. Particle tracking shows that simply melting the continuous Pt film into discrete Pt nanoparticles drastically reduced its speed by ~80% (from ~4.8 μm/s to ~1.3 μm/s). Note that throughout this study, motor speeds were acquired by fitting their mean squared displacement to minimize the effect of Brownian motion (see the Experimental Section for details on the calculation of MSD and fitting).

On the other hand, annealing the Pt film does NOT reduce its catalytic activity, confirmed in Figure 1c by measuring the rate of oxygen evolution (see the Experimental Section and Supporting Information for details) for Pt films both before and after annealing (Video S2 and Video S3). In fact, the catalytic activity of Pt nanoparticles was even ~50% higher than the Pt film they originated from, possibly because of a higher surface area associated with nanoparticles or a cleaner surface after thermal treatment. This enhancement in catalytic activity makes its poor self-propulsion even more surprising.

Weak Propulsion of a SiO_2–Pt_{np} Particle Is Related to Its Surface Morphology. A sharp decrease in motor speeds after annealing was observed for samples fabricated with a range of Pt thickness or annealed at different temperatures. However, Figure 2 reveals that SiO_2–Pt particles with a thicker Pt layer (Figure 2a,b and Video S4) or by annealing the Pt film at a lower temperature (Figure 2c,d and Video S5) contained coarsened Pt islands and moved faster than those made otherwise containing discrete Pt nanoparticles. We again confirm in Figure 2b,d that the significant differences in propulsion among various samples cannot be attributed to the differences in their catalytic activity. Instead, annealed samples often show better catalytic activity (blue data to the right y axis) but worse propulsion (red data) than their unannealed counterparts.

Catalase Does Not Power Micromotors. The poor propulsion of Janus microspheres described above is not limited to the material Pt but likely applies more generically to any system involving the catalytic decomposition of H_2O_2. To showcase this generalizability, we next present results of SiO_2 microspheres asymmetrically decorated with catalase, an enzyme that converts H_2O_2 rapidly into water and O_2 at a turnover rate of $\sim 10^5$ molecule per second.[33,34] Because catalase is comparable to the most active Pt in its catalytic performance, one would naively expect a SiO_2-catalase Janus micromotor to self-propel in the same way as a SiO_2–Pt motor.[35−39] Indeed, there have been reports of nanospheres (100−400 nm in diameters from one group[21,22] and 700 nm in another[23]) half-functionalized with catalase exhibiting enhanced diffusion in the presence of H_2O_2. However, there is curiously no report of catalase-driven Janus micromotors showing directional, phoretic motion in the micrometer scale. (Note that catalase-functionalized motors that are even larger[24] or confined in a tube,[25] on the other hand, will likely produce oxygen bubbles and thus move with a different mechanism that falls outside of the scope of this article. Micromotors powered by other enzymes, such as urease,[23,40] often produce ionic species and are therefore distinct from the case of catalase.) This surprising lack of a report of catalase-laden micromotors has confused us for a long time, and we have convinced ourselves in the past that enzymes, unlike inorganic catalysts, are harder to handle and might be in a poor condition in an experiment.

However, we may now attribute this lack of success to the intrinsic inability of catalase to propel micrometer-scale motors, for the same reason that a SiO_2–Pt_{np} motor cannot,

https://doi.org/10.1021/jacs.1c04501
J. Am. Chem. Soc. 2021, 143, 12154−12164

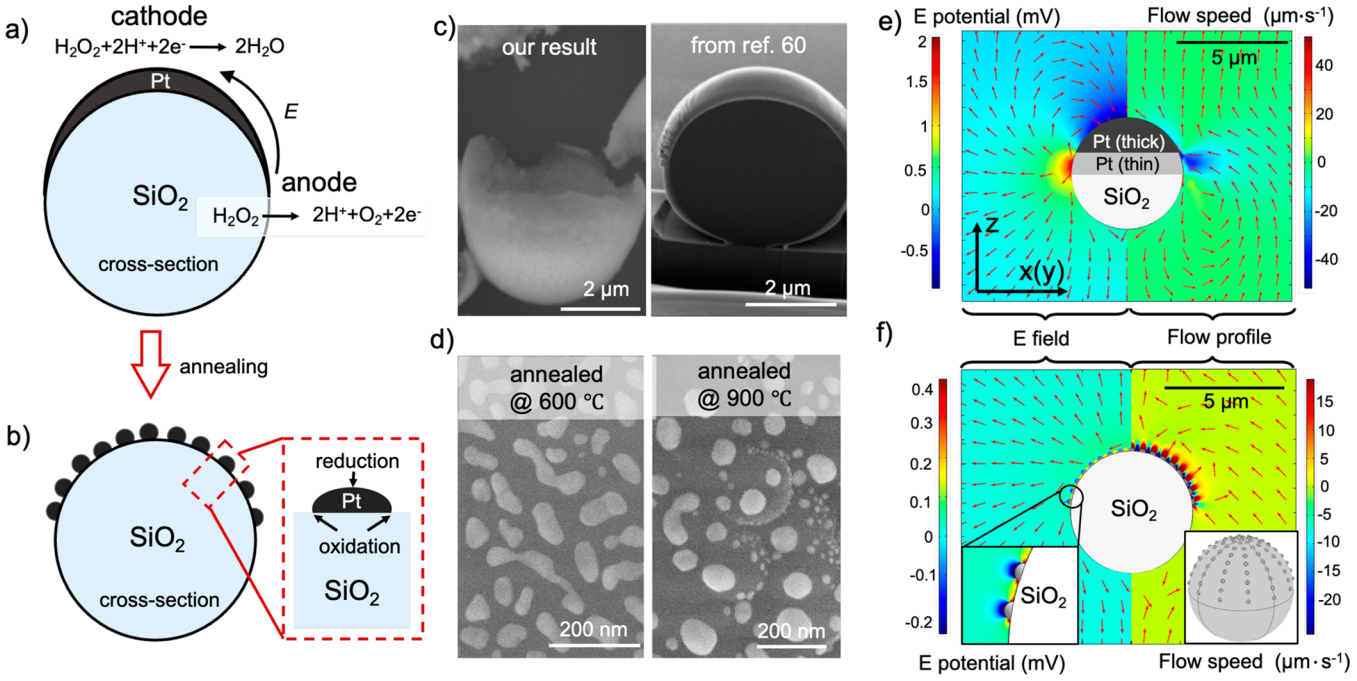

Figure 4. Self-electrophoresis of SiO_2−Pt microspheres. (a) Tentative scheme of the operation of self-electrophoresis on a SiO_2−Pt_{film} micromotor in H_2O_2, with its pole serving as the cathode and the equator as the anode. A self-generated electric field points from the equator to the pole, propelling it away from the Pt cap. (b) For a SiO_2−Pt_{np} microsphere, self-electrophoresis could still occur as a result of the tapered shape of each nanoparticle formed on the surface of the SiO_2 sphere. (c) Scanning electron micrographs of the tapered Pt cap from physical deposition, acquired in our own lab (left, after removing the solid core underneath a Pt coating) and from ref 60 (right, acquired by slicing a Janus microsphere with focused ion beams. Reprinted with permission from ref 60. Copyright 2018, American Chemical Society). (d) Scanning electron micrographs of Pt nanoparticles after annealing a Pt film at 600 or 900 °C. (e and f) Numerical simulations of a SiO_2−Pt_{film} or SiO_2−Pt_{np}. Simulation results of the electrostatics (electrical potential and electric field lines) are shown on the left and stitched with the results from the fluid dynamics (flow speeds along the z direction and normalized flow vectors) on the right. The bottom left inset in part f shows the zoomed-in results of the electric potential near two Pt nanoparticles. The bottom right inset shows the geometric configuration of the model, where a total of 93 Pt nanoparticles of 200 nm in diameter are arranged in concentric circles on one-half of a SiO_2 microsphere. Notably, the simulated speed is ∼5.7 μm/s for a SiO_2−Pt_{film} and ∼0.1 μm/s for a SiO_2−Pt_{np} with the same simulation parameters, because fluid flows in part f are highly localized. See the Supporting Information for modeling details.

as we have amply described above. This argument is supported by three pieces of evidence. First, an early study from the Sanchez lab found the spatial distribution of enzymes (urea to be specific) on a mesoporous SiO_2 microsphere to be heterogeneous and discrete,[41] suggesting that a SiO_2-catalase Janus microsphere is similar to SiO_2−Pt_{np} in surface morphology (note that self-propulsion is not guaranteed even if enzymes were a continuous film because of the absence of electrochemical currents. See below for explanation.). Second, an early experiment from the Sen and the Mallouk lab showed that a microrod asymmetrically functionalized with catalase only showed Brownian motion in H_2O_2.[42] In fact, they clearly stated that "the nonelectrochemical decomposition of H_2O_2 does not contribute significantly to propulsion", a message we also agree but has unfortunately failed to resonate within the community over the years.

Third and finally, our own experiments confirm that SiO_2 microspheres half-functionalized with catalase do not self-propel in H_2O_2 up to 10 wt % (corresponding to 2.9 mol/L). Briefly, SiO_2 microspheres were first functionalized with amine groups on their entire surfaces, followed by physical deposition of gold to block half of the surface. Catalase was then functionalized on the unblocked half. See Figure 3a for fabrication schemes and the Experimental Section for fabrication details. The dynamics of these SiO_2-catalase microspheres in H_2O_2 of a range of concentrations are shown in Video S6 and again presented as tracked trajectories in Figure 3d. Moreover, their MSD plots and diffusivities are given in Figures S6 and S8 (all been corrected for possible drift, see Figure S8), which show a small decrease in diffusivity after enzyme functionalization, possibly because of the weak sticking between enzymes and the substrate.

A series of characterization confirm that the poorly motile SiO_2-catalase microspheres catalyze the decomposition of H_2O_2 actively and asymmetrically (see Experimental Section and Supporting Information for details). First, the successful functionalization of catalase on one side of a SiO_2 microsphere was confirmed by confocal laser scanning microscopy in Figure 3b, which shows that only half of the microsphere is bright (catalase in this case is labeled with fluorescein isothiocyanate, or FITC, a fluorescent dye). Moreover, we experimentally determined the average number of catalase exposed on a Janus SiO_2 microsphere to be ∼2.2×10^6/particle, close to the theoretical estimate of 1.4×10^6 enzymes per particle assuming compact coverage (see the Supporting Information for an estimate).

Second, the catalytic activity of a SiO_2-catalase microsphere was confirmed. This was first qualitatively examined from the production of oxygen bubbles in a cuvette filled with catalase-functionalized SiO_2 particles suspended in H_2O_2 (Figure 3c). More quantitatively, by measuring the oxygen production rate of a catalase-functionalized glass slide in 10 wt % H_2O_2, we

https://doi.org/10.1021/jacs.1c04501
J. Am. Chem. Soc. 2021, 143, 12154−12164

obtained a surface flux of O_2 of 8.3 mmol m^{-2} s^{-1}, comparable to that from a Pt-coated surface reported in Figures 1 and 2 (~10 mmol m^{-2}·s^{-1} for Pt of 5 nm). By connecting this number to the enzyme coverage we determined above, we find that catalase operates on a Janus SiO_2 microsphere at a turnover rate of 8.9×10^4 s^{-1}, smaller than expected from catalase (2.1×10^5 s^{-1}).[33] This reduced enzyme activity is reasonable, given our experiments were conducted at room temperature and in deionized water mixed with a high concentration of H_2O_2, rather than the optimal condition for enzymes at 37 °C in PBS buffers.

DISCUSSION

Brief Survey of Operating Mechanisms. The self-propulsion (or not) of a Pt-coated micromotor is naturally linked to its operating mechanism. Yet, despite the simplicity in its design, fabrication, operation, and motion dynamics (see ref 10 for an overview), the propulsion mechanism of Pt-coated micromotors remains unsettled.[43−47] In the early years, a mechanism of "neutral self-diffusiophoresis" was proposed and widely cited (see, e.g., 48), which states that the Janus particle is driven by a concentration gradient of neutral solutes, most likely O_2, that is generated around the Pt cap as a result of the decomposition of H_2O_2. However, the recent discovery that Pt coated micromotors slow down in solutions of high ionic strength suggests the dominance of electrokinetics.[43−45] As a result, alternative mechanisms have been proposed that emphasize on charged intermediate species,[43,44] an uneven Pt cap that gives rise to self-electrophoresis,[43,44] or more recently local momentum transfer from chemical reactions[49] and ions released.[50] Because Pt Janus micromotors are widely studied as model systems in numerous scenarios, a lack of clear operating mechanism greatly hinders our understanding of how they interact with neighbors or with complex environments[51−54] or how collective behaviors emerge.

Our Results Are Consistent with a Self-Electrophoresis Mechanism. One plausible explanation for our observations that Pt nanoparticles or catalase do not propel a Janus micromotor, but one with a continuous Pt film does, is the self-electrophoresis mechanism recently proposed for a Pt-coated micromotors.[43,44] The key idea of this mechanism is that the decomposition of H_2O_2 on a catalytic surface goes through both a nonelectrochemical and an electrochemical pathway, with the latter split into cathodic and anodic half reactions. Reference 55 confirmed the coexistence of these two pathways. A possible origin for the electrochemical pathway is the heterogeneous morphologies of a Pt film, such as a variation in its roughness or thickness, that favors the oxidation or reduction of H_2O_2 on different spots. The electrochemical decomposition of H_2O_2 generates a proton gradient and consequently an electric field that points from the anode to the cathode, propelling an electrically charged microswimmer in a way similar to the classic example of synthetic microswimmers, a bimetallic microrod moving in H_2O_2, where the self-electrophoresis mechanism was first identified.[42,55−59]

We describe below how the three key ingredients in this self-electrophoresis mechanism, namely a difference in surface morphology of a Pt film, an electrochemical current flowing within it, and an electrophoretic mobility, are all found (albeit with different levels of confidence) for a SiO_2−Pt_{film} micromotor but not for a SiO_2−Pt_{np}.

First, we confirm that a continuous Pt cap on a SiO_2 microsphere displays a variation in its thickness (Figure 4a). A common source of such variation is the physical deposition process from which a Janus microsphere is made, where metals are deposited from above and therefore more on the poles of microspheres and less on their equators. Examples of a tapered Pt cap as a result of this process have been found in the literature[60] and obtained in our lab, as shown in Figure 4c.

Brown et al. and Ebbens et al. further argued[43,44,46] that the catalytic reactivity of the Pt coating was sensitive to its thickness. They showed how a thicker Pt film generated more oxygen than a thinner one[44] and speculated that the thicker region of the Pt film at a pole of a microsphere served as the cathode while the thinner region at the equator as the anode. Although there is no obvious reason why a more catalytically active spot on a Pt film would serve as a cathode, once the designation of electrodes is set, the oxidation and reduction half reactions of H_2O_2 then occurs preferentially on the anode (equator) and the cathode (pole).[46,61] The tapered Pt cap essentially then operates as a battery in short circuits, generating an electrochemical current that moves the micromotor away from its Pt cap.

We then set out to fill the gap in the above reasoning by measuring if there is any electrochemical current flowing between two pieces of Pt films of different thickness in H_2O_2 and which way it flows toward. Electrochemical measurements (see Supporting Information and Figure S9 for details) indeed show currents flowing from the thinner film to the thicker one, conforming to the designation of the cathode and anode proposed from the literature and thus to the self-electrophoresis mechanism. However, the electrical current values recorded were on the order of 1 $\mu A/cm^2$ (Figure S10, corresponding to a surface flux of H^+ on the order of 10^{-7} mol/(m^2 s)), close to a baseline value of 0.2 $\mu A/cm^2$ and 1 order of magnitude smaller than that required to move a micromotor at a speed measured experimentally (see the Supporting Information for an estimate). More efforts are needed in the future to confidently relate this electrochemical current to self-propulsion of a micromotor.

Assuming this proposed mechanism of asymmetric, electrochemical decomposition of H_2O_2 on a Pt film, and assuming that thicker Pt serves as the cathode and the thinner Pt as the anode, we then performed a simple numerical simulation (Figure 4e) that indeed shows how a SiO_2−Pt_{film} microsphere, with its pole set as the cathode and the equator as the anode, is capable of moving away from the Pt cap. Specifically, it moves at a speed of 5.7 μm/s under experimentally relevant parameters such as a zeta potential of −22 mV and a surface flux on the order of 10^{-6} mol/(m^2 s) (see the Supporting Information for simulation details). Although this simulation does not grant much mechanistic insight beyond what is hypothesized above, it shows that this self-electrophoresis mechanism is capable of propelling a micromotor at a speed comparable with experimental values. This piece of numerical evidence completes our reasoning of a self-electrophoresis mechanism.

As another piece of evidence consistent with self-electrophoresis for a Pt-coated microswimmer, we have fabricated a Pt shell by removing the SiO_2 microsphere underneath a sputtered Pt film. Figure 4c and Figure S17b shows how this shell is thin on its edge and thick at the top, and Video S7 shows that this tapered Pt shell moves toward its opening side in H_2O_2. This observation is consistent with a numerical prediction based on self-electrophoresis (Figure S18), even

https://doi.org/10.1021/jacs.1c04501
J. Am. Chem. Soc. 2021, 143, 12154−12164

though it can potentially be explained by other mechanisms as well.

Self-Electrophoresis Breaks down for a SiO_2−Pt_{np}. If a SiO_2−Pt_{film} motor with a continuous Pt film moves well via self-electrophoresis, how does it fail for a motor with discrete Pt nanoparticles? We offer two possible scenarios why this might occur (simulation results in Figure 4f). In the first possibility, as illustrated in Figure 4b, we assume that each discrete Pt nanoparticle is also tapered in a way similar to a much larger Pt cap. This shape could originate from how the Pt film partially melts upon annealing, forming tapered nanoislands when solidified (e.g., Figure 4d, left). For the same reason as a large tapered Pt cap, each of these tapered Pt nanoislands generate their own electric and flow fields but only canceling each other locally, leaving weak global flows around the entire microsphere. Simulation in Figure 4f shows flow speeds and an electric field strength 1 order of magnitude smaller than those generated by a SiO_2−Pt_{film} motor of a continuous Pt cap (Figure 4e) and a speed of 0.1 μm/s for a SiO_2−Pt_{np} versus that of ∼5.7 μm/s for a SiO_2−Pt_{film}, despite a similar turnover rate in both cases.

The second possibility that links self-electrophoresis with the poor propulsion of a SiO_2−Pt_{np} motor is the scenario where the Pt film completely melts into Pt droplets that do not wet the SiO_2 surface. As a result, Pt nanospheres of little taper are formed when cooled. Because the self-electrophoresis mechanism described above requires a separation of the cathode and anode, and thus regions of different thickness, a Pt nanosphere of little taper generates little electrochemical current and consequently minimum speed for the SiO_2−Pt_{np} micromotors. This scenario of nonwetting Pt is perhaps most relevant to samples annealed at high temperatures (e.g., Figure 4d, right), where Pt nanoparticles clearly show a spherical shape (see Figures S11 and S12 for quantification). Similar structures with spherical Pt nanoparticles after annealing have been reported in ref 18.

To use this self-electrophoresis mechanism to justify the results described in Figure 2 (varying Pt thickness and annealing temperatures), we postulate that annealing Pt films at different temperatures, or depositing Pt of different thickness, creates a Pt film with morphologies of varying thickness, degree of tapering, and degree of connectiveness. These morphological factors are intricately related to a surface reactivity, which leads to various degrees of separation of cathode and anode and ultimately different speeds.

Self-electrophoresis could fail for catalase for two reasons. First, it is not clear whether catalase at different spots on a SiO_2 microsphere could exhibit different activity or how this difference could split the decomposition of H_2O_2 into anodic and cathodic half-reactions. Second, even if these half-reactions do occur, there is no conductive pathway that shuttles electrons across two electrodes because catalase, unlike Pt, is poorly electrically conductive.

To close this section, we note that the consistency between our observations and the self-electrophoresis mechanism should not be boldly interpreted as a proof that self-electrophoresis is the dominant mechanism for a Pt-coated microswimmer, because of a lack of direct evidence such as the electrochemical currents on a Pt cap of a Janus microsphere (rather than that between two pieces of Pt films) and the measurement of the proton distributions near a SiO_2−Pt_{film} or a SiO_2−Pt_{np} motor. These measurements are technically challenging at this moment.

Possible Contributions from Other Propulsion Mechanisms. Our observations also offer insight into other potential propulsion mechanisms that may or may not contribute. For example, a popular mechanism for this particular type of microswimmer is self-diffusiophoresis, the self-propulsion from self-generated solute (neutral or ionic) gradient.[2,56,57,62−66] In particular, neutral self-diffusiophoresis could arise from the concentration gradient of O_2 that is higher or of H_2O_2 that is lower near the Pt side as it catalyzes the decomposition of H_2O_2. However, recent theoretical studies of neutral self-diffusiophoresis have suggested that it is a very weak effect,[44,61] and its operation has further been questioned by the quenched mobility in solutions of high salt concentrations,[43−45] as we confirm in our own experiment in Figure S13. (We have noticed the recent experimental study from the Kraft lab,[67] which suggested the possibility of the operation of neutral self-diffusiophoresis despite a salt-dependent speed. However, we remain doubtful over this possibility because of a lack of direct experimental evidence.)

It is also possible for a Pt micromotor to be powered by ionic self-diffusiophoresis,[43,45] arising from charged intermediates, such as OOH^- or radicals, that could be generated by the chemical decomposition of H_2O_2. Phenomelogically, ionic self-diffusiophoresis is challenging to be ruled out, since a motor powered by either it or self-electrophoresis is visually indistinguishable from the other. More importantly, because both self-electrophoresis or ionic self-diffusiophoresis involve charged species and produce a self-generated electric field, a SiO_2−Pt_{film} motor powered by either mechanism would slow down in salt in the same way.

To examine the possible contribution of ionic self-diffusiophoresis in powering either a SiO_2−Pt_{film} or a SiO_2−Pt_{np} micromotor, we have conducted numerical simulations that show in Figure S16 similar speeds between these two motors if ionic self-diffusiophoresis were the propulsion mechanism, contrary to our experiments. In the Supporting Information, we offer an expanded discussion of why this mechanism does not break down for SiO_2−Pt_{np}, despite a clear change in surface morphology and material asymmetry. However, a more accurate assessment would require a better theoretical understanding of how diffusiophoresis is affected by the surface morphologies of a colloidal particle, an important topic that has been rarely explored so far.

We further argue that data in Figure 2b,d quantitatively reveal the minor contributions of diffusiophoresis in powering micromotors, as the Pt film is broken into smaller pieces so that the electrophoretic propulsion diminishes. For example, the results in Figure 2d superficially suggest that ∼80% of the overall speed of a SiO_2−Pt motor comes from self-electrophoresis, with the remaining 20% from self-diffusiophoresis (ionic or neutral).

One could also argue for bubble propulsion,[68] a possibility that arises from the fast generation of O_2 as H_2O_2 decomposes on highly active catalyst such as Pt or catalase. Although large amounts of O_2 bubbles have indeed been observed in our measurements of O_2 evolution, we note that in a typical motor experiment of ours these bubbles nucleated and grew exclusively on the surface of a container, rather than on a microsphere (a scenario more likely for larger motors, see ref 48). Thus, the presence of bubbles did not affect the dynamics of a Pt- or catalase-functionalized microsphere in our experiments. In addition, any drift caused by the growth or burst of bubbles has been corrected.

https://doi.org/10.1021/jacs.1c04501
J. Am. Chem. Soc. 2021, 143, 12154−12164

Finally, we comment on the relevance (or irrelevance) of two recently proposed propulsion mechanisms in understanding our observations. The first mechanism proposed by Corato et al. highlights the importance of the surface flux of ions of different diffusivity.[50] Given that this mechanism "originates entirely from the surface flux of ions, which couples transport of species and the balance of charges", it is likely to be insensitive to the surface morphology as long as the same amount of ions are produced, which is the case between a SiO_2−Pt_{film} and a SiO_2−Pt_{np}. (Note that this ion flux mechanism is likely consistent with the immobility of catalase-coated microspheres because of a lack of apparent ions from its reaction.) A second mechanism, proposed by Eloul et al.,[49] considers the momentum transfer between solvent and colloid and "excludes self-phoretic transport by design". Because this mechanism ultimately comes down to the energy released from the surface catalysis that is powering the momentum transfer, it is likely to be insensitive to the surface morphology as long as the same amount of energy is released. To summarize, although these two mechanisms must involve microscopic details that are sensitive to surface morphology, this is not explicit in either model, and we doubt it explains the 80% drop of speed we see after annealing a thin Pt film into discrete nanoparticles.

Reconciliation with Existing Literature. Our observation that discrete Pt nanoparticles cannot propel micromotors is in seeming disagreement with a number of experimental reports in the literature that show how this can be done. However, this inconsistency can be reconciled by the possible existence of nanobubbles or self-electrophoresis. For example, the Daniela lab has reported that stomatocyte-shaped polymer vesicles loaded with Pt nanoparticles self-propel in H_2O_2,[19,20] while mentioning the possibility of oxygen nanobubbles as a result of Pt-catalyzed decomposition of H_2O_2 within the polymer cavity. In addition, the Ozin lab reported the self-propulsion in H_2O_2 of a sphere dimer consisting of a silica microsphere and one Pt nanoparticle 300−500 nm in diameter,[18] yet no mechanism was explicitly given. We suspect the possible role of nanobubbles in the same spirit as in the case of stomatocytes as well as possible self-electrophoresis as a result of the imperfect shape (and therefore possible differences in activity) of the formed Pt nanoparticles, as the authors noted. In summary, we do not see any literature report of the same SiO_2−Pt_{np} microspheres as those described in the current study that can self-propel in H_2O_2. Nor did we find any evidence that self-diffusiophoresis is unambiguously the dominant mechanism for a Pt-coated nano- or microswimmer.

When comparing our results with the existing literature, one cannot help but wonder if the motor size is an important factor in selecting its propulsion mechanism. For example, as we listed in an earlier section, there have been a few early studies showing enhanced diffusion of catalase-functionalized nanomotors, even though our experiments show their micrometer-counterparts do not self-propel. Similarly, the examples of motors we discussed in the last paragraph are all in the nanometer scale and therefore suggest a difference in the effectiveness of certain propulsion mechanisms operating at different scales (see ref 48 for how two mechanisms crossover as motor sizes increase). In the current case, it is an open possibility that, at the nanometer scale, self-diffusiophoresis, reactive momentum transfer, or ion fluxes become a completely viable mechanism while self-electrophoresis fails because of an inefficient separation of the cathode and anode. Understanding this crossover is an exciting research topic for the future.

CONCLUSION

To conclude, the main message of this study is that, contrary to intuition, the nonelectrochemical decomposition of H_2O_2, one that does not involve a spatial separation of cathodic and anodic half reactions, does NOT lead to effective self-propulsion at the micrometer scale, even if it occurs strongly and asymmetrically on the particle. This argument is supported by evidence in both nonbiological and biological systems: both Pt nanoparticles and catalase rapidly decompose H_2O_2 into water and O_2, but neither propels the corresponding Janus microspheres significantly beyond Brownian motion. A typical result is that annealing the Pt film half-coated on a SiO_2 microsphere reduces its propulsion speed by ∼80%, despite a mild increase in the catalytic reactivity.

These experimental results are aligned with a self-electrophoresis mechanism, possibly arising from the electrochemical decomposition of H_2O_2 on a Pt cap of varied thickness. This mechanism is supported by examining the morphology of a Pt cap, by measuring the electrochemical current flowing between Pt films of different thickness, and by numerical simulations that yield speeds comparable to experimental values. Annealing the Pt film, however, breaks the film into small circuits that cancel each other, or produces Pt nanospheres without any cathode or anode. The operation of self-electrophoresis is unlikely for a catalase-laden micromotor.

On the other hand, our observations are in seeming disagreement with other mechanisms such as self-diffusiophoresis, reactive momentum transfer, or ion fluxes. One route of resolving this inconsistency is to look more closely at how surface morphology changes these mechanisms. The other possibility is that, for reasons unknown, they are more effective for powering nanoscopic swimmers but not those at the micrometer scale.

This study is a key piece of the puzzle in elucidating how chemical reactions power nano- or microscopic objects,[69−71] which is in turn critical for understanding their collective behaviors and dynamic self-assembly,[72] or in complex environments, where whether an electric field surrounds each particle could lead to completely different interpretations and designs.[51−53,73] Finally, our findings could offer new insight in the emerging topic of enzymes or reacting molecules as active matter[39,74,75] and that of harnessing enzymes to do useful work.[37]

ASSOCIATED CONTENT

Supporting Information

The Supporting Information is available free of charge at https://pubs.acs.org/doi/10.1021/jacs.1c04501.

Details on experiments and finite element simulations (PDF)

Video S1, SiO_2−Pt_{film} and SiO_2−Pt_{np} Janus microspheres moving in 10 wt % H_2O_2 (MP4)

Video S2, catalytic activity of Pt films (MP4)

Video S3, measurement of O_2 evolution rate (MP4)

Video S4, effect of film thickness on motor dynamics (MP4)

Video S5, effect of annealing temperatures on motor dynamics (MP4)

Video S6, SiO_2-catalase microspheres in H_2O_2 (MP4)

https://doi.org/10.1021/jacs.1c04501
J. Am. Chem. Soc. 2021, 143, 12154−12164

Video S7, Pt shells moving in 5 wt % H_2O_2 (MP4)

AUTHOR INFORMATION

Corresponding Authors

Xing Ma − *School of Materials Science and Engineering, Harbin Institute of Technology (Shenzhen), Shenzhen, Guangdong 518055, China; Sauvage Laboratory for Smart Materials, Harbin Institute of Technology (Shenzhen), Shenzhen 518055, China; Shenzhen Bay Laboratory, Shenzhen 518055, China;* orcid.org/0000-0002-2248-4806; Email: maxing@hit.edu.cn

Wei Wang − *School of Materials Science and Engineering, Harbin Institute of Technology (Shenzhen), Shenzhen, Guangdong 518055, China;* orcid.org/0000-0003-4163-3173; Email: weiwangsz@hit.edu.cn

Authors

Xianglong Lyu − *School of Materials Science and Engineering, Harbin Institute of Technology (Shenzhen), Shenzhen, Guangdong 518055, China*

Xiaoxia Liu − *School of Materials Science and Engineering, Harbin Institute of Technology (Shenzhen), Shenzhen, Guangdong 518055, China; Sauvage Laboratory for Smart Materials, Harbin Institute of Technology (Shenzhen), Shenzhen 518055, China*

Chao Zhou − *School of Materials Science and Engineering, Harbin Institute of Technology (Shenzhen), Shenzhen, Guangdong 518055, China*

Shifang Duan − *School of Materials Science and Engineering, Harbin Institute of Technology (Shenzhen), Shenzhen, Guangdong 518055, China*

Pengzhao Xu − *School of Materials Science and Engineering, Harbin Institute of Technology (Shenzhen), Shenzhen, Guangdong 518055, China*

Jia Dai − *Department of Chemistry, The University of Hong Kong, Hong Kong 999077, China*

Xiaowen Chen − *School of Materials Science and Engineering, Harbin Institute of Technology (Shenzhen), Shenzhen, Guangdong 518055, China*

Yixin Peng − *School of Materials Science and Engineering, Harbin Institute of Technology (Shenzhen), Shenzhen, Guangdong 518055, China*

Donghao Cui − *School of Materials Science and Engineering, Harbin Institute of Technology (Shenzhen), Shenzhen, Guangdong 518055, China*

Jinyao Tang − *State Key Laboratory of Synthetic Chemistry and Department of Chemistry, The University of Hong Kong, Hong Kong 999077, China;* orcid.org/0000-0002-0051-148X

Complete contact information is available at: https://pubs.acs.org/10.1021/jacs.1c04501

Notes

The authors declare no competing financial interest.

ACKNOWLEDGMENTS

This project is financially supported by the National Natural Science Foundation of China (Grants 11774075 and 52072095), Natural Science Foundation of Guangdong Province (Grant No. 2017B030306005), the Science Technology and Innovation Program of Shenzhen (Grants JCYJ20190806144807401 and KQTD20170809110344233), and Shenzhen Bay Laboratory (Grant SZBL201906281005). We are grateful for the helpful discussions with Steve Ebbens, Huanhuan Feng, Darrel Velegol, Hepeng Zhang, Thomas Mallouk, Jeffrey Moran, and Dr. Marco De Corato and for the code of drift correction from Prof. Himanagamanasa Kandula at UMass. We are also greatly indebted to Mihail Popescu and William Uspal for their insightful and critical comments on the manuscript.

REFERENCES

(1) Chen, X.; Zhou, C.; Wang, W. Colloidal Motors 101: A Beginner's Guide to Colloidal Motor Research. *Chem. - Asian J.* **2019**, *14* (14), 2388−2405.

(2) Wang, W.; Duan, W.; Ahmed, S.; Mallouk, T. E.; Sen, A. Small power: Autonomous nano-and micromotors propelled by self-generated gradients. *Nano Today* **2013**, *8* (5), 531−554.

(3) Mallouk, T. E.; Sen, A. Powering nanorobots. *Sci. Am.* **2009**, *300* (5), 72−77.

(4) Wang, J. *Nanomachines: Fundamentals and Applications*; John Wiley & Sons, 2013.

(5) Gao, W.; Wang, J. Synthetic micro/nanomotors in drug delivery. *Nanoscale* **2014**, *6* (18), 10486−10494.

(6) Pacheco, M.; López, M. Á.; Jurado-Sánchez, B.; Escarpa, A. Self-propelled micromachines for analytical sensing: a critical review. *Anal. Bioanal. Chem.* **2019**, *411* (25), 6561−6573.

(7) Parmar, J.; Vilela, D.; Villa, K.; Wang, J.; Sánchez, S. Micro-and nanomotors as active environmental microcleaners and sensors. *J. Am. Chem. Soc.* **2018**, *140* (30), 9317−9331.

(8) Li, J.; Gao, W.; Dong, R.; Pei, A.; Sattayasamitsathit, S.; Wang, J. Nanomotor lithography. *Nat. Commun.* **2014**, *5*, 5026.

(9) Zhang, J.; Luijten, E.; Grzybowski, B. A.; Granick, S. Active colloids with collective mobility status and research opportunities. *Chem. Soc. Rev.* **2017**, *46* (18), 5551−5569.

(10) Wang, W.; Lv, X.; Moran, J. L.; Duan, S.; Zhou, C. A practical guide to active colloids: choosing synthetic model systems for soft matter physics research. *Soft Matter* **2020**, *16* (16), 3846−3868.

(11) Zöttl, A.; Stark, H. Emergent behavior in active colloids. *J. Phys.: Condens. Matter* **2016**, *28* (25), 253001.

(12) Howse, J. R.; Jones, R. A.; Ryan, A. J.; Gough, T.; Vafabakhsh, R.; Golestanian, R. Self-motile colloidal particles: from directed propulsion to random walk. *Phys. Rev. Lett.* **2007**, *99* (4), 048102.

(13) Ebbens, S. J.; Howse, J. R. Direct observation of the direction of motion for spherical catalytic swimmers. *Langmuir* **2011**, *27* (20), 12293−12296.

(14) Safdar, M.; Wani, O. M.; Jänis, J. Manganese oxide-based chemically powered micromotors. *ACS Appl. Mater. Interfaces* **2015**, *7* (46), 25580−25585.

(15) Gao, Y.; Dullens, R. P.; Aarts, D. G. Bulk synthesis of silver-head colloidal rodlike micromotors. *Soft Matter* **2018**, *14* (35), 7119−7125.

(16) Teo, W. Z.; Wang, H.; Pumera, M. Beyond platinum: Silver-catalyst based bubble-propelled tubular micromotors. *Chem. Commun.* **2016**, *52* (23), 4333−4336.

(17) Shah, Z. H.; Wang, S.; Xian, L.; Zhou, X.; Chen, Y.; Lin, G.; Gao, Y. Highly efficient chemically-driven micromotors with controlled snowman-like morphology. *Chem. Commun.* **2020**, *56* (97), 15301−15304.

(18) Valadares, L. F.; Tao, Y. G.; Zacharia, N. S.; Kitaev, V.; Galembeck, F.; Kapral, R.; Ozin, G. A. Catalytic nanomotors: Self-propelled sphere dimers. *Small* **2010**, *6* (4), 565−572.

(19) Tu, Y.; Peng, F.; Sui, X.; Men, Y.; White, P. B.; van Hest, J. C.; Wilson, D. A. Self-propelled supramolecular nanomotors with temperature-responsive speed regulation. *Nat. Chem.* **2017**, *9* (5), 480−486.

(20) Wilson, D. A.; Nolte, R. J.; Van Hest, J. C. Autonomous movement of platinum-loaded stomatocytes. *Nat. Chem.* **2012**, *4* (4), 268−274.

(21) Ma, X.; Jannasch, A.; Albrecht, U.-R.; Hahn, K.; Miguel-López, A.; Schaffer, E.; Sanchez, S. Enzyme-powered hollow mesoporous Janus nanomotors. *Nano Lett.* **2015**, *15* (10), 7043−7050.
(22) Ma, X.; Sánchez, S. Bio-catalytic mesoporous Janus nanomotors powered by catalase enzyme. *Tetrahedron* **2017**, *73* (33), 4883−4886.
(23) Dey, K. K.; Zhao, X.; Tansi, B. M.; Méndez-Ortiz, W. J.; Córdova-Figueroa, U. M.; Golestanian, R.; Sen, A. Micromotors powered by enzyme catalysis. *Nano Lett.* **2015**, *15* (12), 8311−8315.
(24) Nakata, S.; Nomura, M.; Yamamoto, H.; Izumi, S.; Suematsu, N. J.; Ikura, Y.; Amemiya, T. Periodic Oscillatory Motion of a Self-Propelled Motor Driven by Decomposition of H_2O_2 by Catalase. *Angew. Chem.* **2017**, *129* (3), 879−882.
(25) Xie, Y.; Fu, S.; Wu, J.; Lei, J.; Ju, H. Motor-based microprobe powered by bio-assembled catalase for motion detection of DNA. *Biosens. Bioelectron.* **2017**, *87*, 31−37.
(26) Gao, W.; Pei, A.; Dong, R.; Wang, J. Catalytic iridium-based Janus micromotors powered by ultralow levels of chemical fuels. *J. Am. Chem. Soc.* **2014**, *136* (6), 2276−2279.
(27) Gao, W.; D'Agostino, M.; Garcia-Gradilla, V.; Orozco, J.; Wang, J. Multi-fuel driven janus micromotors. *Small* **2013**, *9* (3), 467−471.
(28) Feng, Y.; Yuan, Y.; Wan, J.; Yang, C.; Hao, X.; Gao, Z.; Luo, M.; Guan, J. Self-adaptive enzyme-powered micromotors with switchable propulsion mechanism and motion directionality. *Appl. Phys. Rev.* **2021**, *8* (1), 011406.
(29) Yang, Y.; Arque, X.; Patiño, T.; Guillerm, V.; Blersch, P.-R.; Pérez-Carvajal, J.; Imaz, I.; Maspoch, D.; Sánchez, S. Enzyme-Powered Porous Micromotors Built from a Hierarchical Micro-and Mesoporous UiO-Type Metal−Organic Framework. *J. Am. Chem. Soc.* **2020**, *142* (50), 20962−20967.
(30) Novotný, F.; Pumera, M. Nanomotor tracking experiments at the edge of reproducibility. *Sci. Rep.* **2019**, *9*, 13222.
(31) Dunderdale, G.; Ebbens, S.; Fairclough, P.; Howse, J. Importance of particle tracking and calculating the mean-squared displacement in distinguishing nanopropulsion from other processes. *Langmuir* **2012**, *28* (30), 10997−11006.
(32) Duan, W.; Ibele, M.; Liu, R.; Sen, A. Motion analysis of light-powered autonomous silver chloride nanomotors. *Eur. Phys. J. E: Soft Matter Biol. Phys.* **2012**, *35*, 77.
(33) Sengupta, S.; Patra, D.; Ortiz-Rivera, I.; Agrawal, A.; Shklyaev, S.; Dey, K. K.; Córdova-Figueroa, U.; Mallouk, T. E.; Sen, A. Self-powered enzyme micropumps. *Nat. Chem.* **2014**, *6* (5), 415.
(34) Sengupta, S.; Dey, K. K.; Muddana, H. S.; Tabouillot, T.; Ibele, M. E.; Butler, P. J.; Sen, A. Enzyme molecules as nanomotors. *J. Am. Chem. Soc.* **2013**, *135* (4), 1406−1414.
(35) Patiño, T.; Arque, X.; Mestre, R.; Palacios, L.; Sánchez, S. Fundamental aspects of enzyme-powered micro-and nanoswimmers. *Acc. Chem. Res.* **2018**, *51* (11), 2662−2671.
(36) Feng, M.; Gilson, M. K. Enhanced diffusion and chemotaxis of enzymes. *Annu. Rev. Biophys.* **2020**, *49*, 87−105.
(37) Zhao, X.; Gentile, K.; Mohajerani, F.; Sen, A. Powering motion with enzymes. *Acc. Chem. Res.* **2018**, *51* (10), 2373−2381.
(38) Ma, X.; Hortelão, A. C.; Patiño, T.; Sánchez, S. Enzyme catalysis to power micro/nanomachines. *ACS Nano* **2016**, *10* (10), 9111−9122.
(39) Ghosh, S.; Somasundar, A.; Sen, A. Enzymes as Active Matter. *Annu. Rev. Condens. Matter Phys.* **2021**, *12*, 177.
(40) Arqué, X.; Andrés, X.; Mestre, R.; Ciraulo, B.; Ortega Arroyo, J.; Quidant, R.; Patiño, T.; Sánchez, S. Ionic Species Affect the Self-Propulsion of Urease-Powered Micromotors. *Research* **2020**, *2020*, 2424972.
(41) Patiño, T.; Feiner-Gracia, N.; Arque, X.; Miguel-López, A.; Jannasch, A.; Stumpp, T.; Schäffer, E.; Albertazzi, L.; Sánchez, S. Influence of enzyme quantity and distribution on the self-propulsion of non-Janus urease-powered micromotors. *J. Am. Chem. Soc.* **2018**, *140* (25), 7896−7903.
(42) Wang, Y.; Hernandez, R. M.; Bartlett, D. J.; Bingham, J. M.; Kline, T. R.; Sen, A.; Mallouk, T. E. Bipolar electrochemical mechanism for the propulsion of catalytic nanomotors in hydrogen peroxide solutions. *Langmuir* **2006**, *22* (25), 10451−10456.
(43) Brown, A.; Poon, W. Ionic effects in self-propelled Pt-coated Janus swimmers. *Soft Matter* **2014**, *10* (22), 4016−4027.
(44) Ebbens, S.; Gregory, D.; Dunderdale, G.; Howse, J.; Ibrahim, Y.; Liverpool, T.; Golestanian, R. Electrokinetic effects in catalytic platinum-insulator Janus swimmers. *EPL (Europhysics Letters)* **2014**, *106* (5), 58003.
(45) Brown, A. T.; Poon, W. C.; Holm, C.; De Graaf, J. Ionic screening and dissociation are crucial for understanding chemical self-propulsion in polar solvents. *Soft Matter* **2017**, *13* (6), 1200−1222.
(46) Campbell, A. I.; Ebbens, S. J.; Illien, P.; Golestanian, R. Experimental observation of flow fields around active Janus spheres. *Nat. Commun.* **2019**, *10*, 3952.
(47) Ibrahim, Y.; Golestanian, R.; Liverpool, T. B. Multiple phoretic mechanisms in the self-propulsion of a Pt-insulator Janus swimmer. *J. Fluid Mech.* **2017**, *828*, 318−352.
(48) Zhang, J.; Zheng, X.; Cui, H.; Silber-Li, Z. The self-propulsion of the spherical Pt−SiO_2 Janus micro-motor. *Micromachines* **2017**, *8* (4), 123.
(49) Eloul, S.; Poon, W. C.; Farago, O.; Frenkel, D. Reactive momentum transfer contributes to the self-propulsion of Janus particles. *Phys. Rev. Lett.* **2020**, *124* (18), 188001.
(50) De Corato, M.; Arqué, X.; Patino, T.; Arroyo, M.; Sánchez, S.; Pagonabarraga, I. Self-propulsion of active colloids via ion release: Theory and experiments. *Phys. Rev. Lett.* **2020**, *124* (10), 108001.
(51) Vutukuri, H. R.; Hoore, M.; Abaurrea-Velasco, C.; van Buren, L.; Dutto, A.; Auth, T.; Fedosov, D. A.; Gompper, G.; Vermant, J. Active particles induce large shape deformations in giant lipid vesicles. *Nature* **2020**, *586* (7827), 52−56.
(52) Katuri, J.; Uspal, W. E.; Simmchen, J.; Miguel-López, A.; Sánchez, S. Cross-stream migration of active particles. *Science Advances* **2018**, *4* (1), eaao1755.
(53) Das, S.; Garg, A.; Campbell, A. I.; Howse, J.; Sen, A.; Velegol, D.; Golestanian, R.; Ebbens, S. J. Boundaries can steer active Janus spheres. *Nat. Commun.* **2015**, *6*, 8999.
(54) Baraban, L.; Harazim, S. M.; Sanchez, S.; Schmidt, O. G. Chemotactic behavior of catalytic motors in microfluidic channels. *Angew. Chem.* **2013**, *125* (21), 5662−5666.
(55) Wang, W.; Chiang, T.-Y.; Velegol, D.; Mallouk, T. E. Understanding the efficiency of autonomous nano-and microscale motors. *J. Am. Chem. Soc.* **2013**, *135* (28), 10557−10565.
(56) Moran, J. L.; Posner, J. D. Phoretic self-propulsion. *Annu. Rev. Fluid Mech.* **2017**, *49*, 511−540.
(57) Aubret, A.; Ramananarivo, S.; Palacci, J. Eppur si muove, and yet it moves: Patchy (phoretic) swimmers. *Curr. Opin. Colloid Interface Sci.* **2017**, *30*, 81−89.
(58) Paxton, W. F.; Baker, P. T.; Kline, T. R.; Wang, Y.; Mallouk, T. E.; Sen, A. Catalytically induced electrokinetics for motors and micropumps. *J. Am. Chem. Soc.* **2006**, *128* (46), 14881−14888.
(59) Paxton, W. F.; Kistler, K. C.; Olmeda, C. C.; Sen, A.; St. Angelo, S. K.; Cao, Y.; Mallouk, T. E.; Lammert, P. E.; Crespi, V. H. Catalytic nanomotors: autonomous movement of striped nanorods. *J. Am. Chem. Soc.* **2004**, *126* (41), 13424−13431.
(60) Rashidi, A.; Issa, M. W.; Martin, I. T.; Avishai, A.; Razavi, S.; Wirth, C. L. Local measurement of Janus particle cap thickness. *ACS Appl. Mater. Interfaces* **2018**, *10* (37), 30925−30929.
(61) Ibrahim, Y.; Golestanian, R.; Liverpool, T. B. Multiple phoretic mechanisms in the self-propulsion of a Pt-insulator Janus swimmer. *J. Fluid Mech.* **2017**, *828*, 318−352.
(62) Zhou, C.; Zhang, H.; Tang, J.; Wang, W. Photochemically powered AgCl Janus micromotors as a model system to understand ionic self-diffusiophoresis. *Langmuir* **2018**, *34* (10), 3289−3295.
(63) Popescu, M. N.; Uspal, W. E.; Dietrich, S. Self-diffusiophoresis of chemically active colloids. *Eur. Phys. J.: Spec. Top.* **2016**, *225* (11), 2189−2206.
(64) Velegol, D.; Garg, A.; Guha, R.; Kar, A.; Kumar, M. Origins of concentration gradients for diffusiophoresis. *Soft Matter* **2016**, *12* (21), 4686−4703.

(65) Anderson, J. L. Colloid transport by interfacial forces. *Annu. Rev. Fluid Mech.* **1989**, *21* (1), 61−99.
(66) Nourhani, A.; Lammert, P. E.; Crespi, V. H.; Borhan, A. A general flux-based analysis for spherical electrocatalytic nanomotors. *Phys. Fluids* **2015**, *27* (1), 012001.
(67) Ketzetzi, S.; de Graaf, J.; Kraft, D. J. Diffusion-based height analysis reveals robust microswimmer-wall separation. *Phys. Rev. Lett.* **2020**, *125* (23), 238001.
(68) Liu, L.; Bai, T.; Chi, Q.; Wang, Z.; Xu, S.; Liu, Q.; Wang, Q. How to make a fast, efficient bubble-driven micromotor: A mechanical view. *Micromachines* **2017**, *8* (9), 267.
(69) Zhang, Y.; Hess, H. Chemically-powered swimming and diffusion in the microscopic world. *Nature Reviews Chemistry* **2021**, *5*, 500−510.
(70) Dey, K. K.; Sen, A. Chemically propelled molecules and machines. *J. Am. Chem. Soc.* **2017**, *139* (23), 7666−7676.
(71) Robertson, B.; Huang, M.-J.; Chen, J.-X.; Kapral, R. Synthetic nanomotors: working together through chemistry. *Acc. Chem. Res.* **2018**, *51* (10), 2355−2364.
(72) Nourhani, A.; Brown, D.; Pletzer, N.; Gibbs, J. G. Engineering contactless particle−particle interactions in active microswimmers. *Adv. Mater.* **2017**, *29* (47), 1703910.
(73) Simmchen, J.; Katuri, J.; Uspal, W. E.; Popescu, M. N.; Tasinkevych, M.; Sánchez, S. Topographical pathways guide chemical microswimmers. *Nat. Commun.* **2016**, *7*, 10598.
(74) Zhang, Y.; Hess, H. Enhanced diffusion of catalytically active enzymes. *ACS Cent. Sci.* **2019**, *5* (6), 939−948.
(75) Wang, H.; Park, M.; Dong, R.; Kim, J.; Cho, Y.-K.; Tlusty, T.; Granick, S. Boosted molecular mobility during common chemical reactions. *Science* **2020**, *369* (6503), 537−541.

https://doi.org/10.1021/jacs.1c04501
J. Am. Chem. Soc. 2021, 143, 12154−12164